

STOCHASTIC DYNAMICS OF KEPLERIAN ACCRETION DISKS

PETROS J. IOANNOU AND ALEXANDER KAKOURIS

Section of Astrophysics, Astronomy and Mechanics, Physics Department, University of Athens, GR 15784 Panepistimiopolis, Athens, Greece;
pji@cc.uoa.gr, akakour@cc.uoa.gr

Received 2000 July 28; accepted 2000 November 16

ABSTRACT

In this work we study the growth of perturbations in Keplerian disks. Despite the asymptotic stability of the disk, a subset of optimal perturbations are found to exhibit large transient growth. The transient growth is due to the nonnormality of the underlying operator which governs the perturbation dynamics. It is shown that the amplifying perturbations produce positive momentum fluxes and a tendency of outward angular momentum expulsion during amplification. We calculate the statistical steady state that emerges under white forcing in space and time. The perturbation structure is found to be organized in coherent structures that invariably export angular momentum outward. The radial structure of the resulting angular momentum flux is in agreement with the predictions of the equilibrium theory of accretion disks. The effect of spatial localization and temporal band limiting of the forcing on the maintained momentum fluxes is investigated. We find that if the forcing is broadband and adequately distributed, accretion to the main body can be maintained by stochastic forcing.

Subject headings: accretion, accretion disks — hydrodynamics — novae, cataclysmic variables

1. INTRODUCTION

Mass accretion in astrophysical accretion disks requires expulsion of angular momentum to the exterior of the disk. Because molecular viscosity in such disks is believed to be very small, the outward angular momentum flux is believed to be produced by turbulent Reynolds stresses requiring that the disks are in a turbulent state (Shakura & Sunyaev 1973; Papaloizou & Lin 1995; Balbus & Hawley 1998; Hawley, Balbus, & Winters 1999; Balbus & Papaloizou 1999). However, the nature of turbulence, especially in astrophysical disks in near-Keplerian rotation, is not known. Generally, Keplerian disks have been found to be asymptotically stable to linearized perturbations of pure hydrodynamic origin, and although weak instabilities exist in Keplerian disks confined between reflecting boundaries (Jaroszyński 1988; Godon 1998) or in Keplerian disks with local regions of non-Keplerian angular velocities (Lovelace et al. 1999; Li et al. 2000), numerical experiments cast a serious doubt on whether Keplerian disks can transition to turbulence by pure hydrodynamic processes (Balbus, Hawley, & Stone 1996; Balbus & Hawley 1998; Hawley et al. 1999). While Keplerian disks are generally asymptotically stable to pure hydrodynamic perturbations, they are unstable to magnetohydrodynamic instabilities (Chandrasekhar 1960; Balbus & Hawley 1991), and it has been argued that the anomalous viscosity required for mass accretion is provided by the magnetohydrodynamic turbulence that develops in ionized disks (Balbus et al. 1996; Balbus & Hawley 1998; Hawley et al. 1999). However, the fraction of ionized matter is often too small to support magnetohydrodynamic turbulence, as, for example, for accretion in binaries during quiescence (Menou 2000). It is therefore necessary to revisit the fundamental processes that can be responsible for inducing accretion in Keplerian disks by pure hydrodynamic processes.

The study of the stability of Keplerian accretion disks has been largely limited to eigenanalysis of the operator linearized about the mean state of Keplerian rotation. However, Keplerian disks can exhibit transient energy growth despite their asymptotic stability (Goldreich & Lynden-Bell 1965;

Toomre 1964, 1981), which reveals that the perturbation dynamics are governed by a nonnormal operator (an operator A is nonnormal when it does not commute with its adjoint A^\dagger). Nonnormal operators have nonorthogonal eigenfunctions in any physically useful inner product, like the perturbation energy, and eigenanalysis reveals only the large time behavior of the perturbation dynamics and gives little information about the dynamical evolution of perturbation structure for times of the order of the rotational period of the disk. Moreover, in nonnormal systems the fluxes associated with the eigenmodes do not necessarily reveal the structure of the eddy fluxes when the flow is excited by general initial conditions, and the momentum transport is determined by the structure of the growing perturbations. In order to address the behavior of perturbations at short times one must resort to the methods of generalized stability analysis that can reveal the growth potential of perturbations in the flow, their structure, and associated eddy fluxes (Farrell & Ioannou 1996, 1999a, 1999b).

In this work we present a generalized stability analysis of Keplerian disks. We concentrate on the question of whether the disk when stochastically forced can produce observed levels of outward angular momentum transport as inferred from observations of the radiated power. Stochastic forcing of the large scales represents either external forcing of the disk (tidal forcing, shock wave debris, outbursts) or internal forcing by the nonlinear terms, if the disk is indeed in a turbulent state (Farrell & Ioannou 1999b). Parameterization of the nonlinear Jacobian in shear turbulence by an unstructured stochastic forcing has been previously shown to produce the observed structure of the eddy fields in laboratory shear turbulence (Farrell & Ioannou 1993a, 1993c, 1998) and of the transient eddy fluxes of the atmosphere at the midlatitudes (Farrell & Ioannou 1995).

In this paper we consider flat two-dimensional Keplerian disks of constant density in which the effects of self-gravity are neglected in the perturbation dynamics. Besides the above simplifying assumptions, we make also the simplifying assumption that the magnitude of the substantial time

derivatives of the eddy fields are small compared to the rotational frequency of the disk. In that case the eddy fields are rotationally balanced, the perturbations are quasi-nondivergent, and the perturbation dynamics conserve potential vorticity. The perturbation dynamics under these assumptions have the same qualitative character with incompressible dynamics. For simplicity we treat here the case of a Keplerian disk with strictly nondivergent eddy fields. The character of turbulence in compressible accretion disks is presently unknown, and the degree of dominance of rotationally balanced eddy motions in the turbulent state is presently under investigation.

2. EVOLUTION OF PERTURBATIONS IN A SIMPLE KEPLERIAN DISK

We consider a two-dimensional incompressible disk of constant surface density Σ rotating around a central massive body M . The disk's mean state is radially symmetric with mean velocity $[U(r), r\Omega(r)]$, where $U(r)$ is the mean radial inflow and $r\Omega(r)$ the azimuthal, θ , velocity component. The mean angular velocity is considered Keplerian,

$$\Omega(r) = \Omega_0(r_0/r)^{3/2}, \quad (1)$$

where r_0 is the radial distance from the central massive body at which the centrifugal acceleration balances the gravitational acceleration, i.e., $r_0 = (GM/\Omega_0^2)^{1/3}$. We neglect self-gravity but consider the disk viscous with coefficient of kinematic viscosity ν . The viscous stress from the mean differential rotation is balanced by the mean inflow velocity, $U(r)$, which is determined from the azimuthal momentum equation:

$$U(r) \frac{d(r^2\Omega)}{dr} = \nu r \frac{d}{dr} \left[\frac{1}{r} \frac{d(r^2\Omega)}{dr} \right], \quad (2)$$

which gives for Keplerian angular velocity the mean inflow:

$$U(r) = -\frac{3\nu}{2r}. \quad (3)$$

Small velocity departures from the mean state $[u(r, \theta, t), v(r, \theta, t)]$, where u is the radial and v the azimuthal (zonal) perturbation velocity, obey the linearized vorticity equation:

$$\left[\frac{\partial}{\partial t} + \Omega(r) \frac{\partial}{\partial \theta} + U(r) \frac{\partial}{\partial r} - \nu \nabla^2 \right] \zeta = -\frac{dZ(r)}{dr} u, \quad (4)$$

where ζ is the perturbation vorticity

$$\zeta = \frac{1}{r} \left[\frac{\partial(rv)}{\partial r} - \frac{\partial u}{\partial \theta} \right], \quad (5)$$

Z the vorticity of the mean flow

$$Z(r) = \frac{1}{r} \frac{d(r^2\Omega)}{dr} = \frac{1}{2} \Omega(r), \quad (6)$$

and ∇^2 the Laplacian operator in polar coordinates

$$\nabla^2 \equiv \frac{\partial^2}{\partial r^2} + \frac{1}{r} \frac{\partial}{\partial r} + \frac{1}{r^2} \frac{\partial^2}{\partial \theta^2}. \quad (7)$$

Because the perturbations are considered incompressible, the perturbation velocities can be determined from a stream

function ψ

$$u = -\frac{1}{r} \frac{\partial \psi}{\partial \theta}, \quad v = \frac{\partial \psi}{\partial r}, \quad (8)$$

and, consequently, the perturbation vorticity becomes $\zeta = \nabla^2 \psi$, from which the velocities can be determined if the vorticity field is given and boundary conditions are imposed.

Consider now the evolution of harmonic perturbations of the form $\psi(r, \theta, t) = \hat{\psi}(r, t) e^{im\theta}$, $\zeta(r, \theta, t) = \hat{\zeta}(r, t) e^{im\theta}$ where m is the azimuthal wavenumber. The perturbation evolution equation (4) takes the form

$$\frac{d\hat{\zeta}}{dt} = -im\Omega(r)\hat{\zeta} - U(r) \frac{d\hat{\zeta}}{dr} + i \frac{m}{2r} \frac{d\Omega(r)}{dr} (D^2)^{-1} \hat{\zeta} + \nu D^2 \hat{\zeta}, \quad (9)$$

having written $\hat{\psi} = (D^2)^{-1} \hat{\zeta}$. Ω is the Keplerian angular velocity given by equation (1), the inflow velocity U is given by equation (3), and the Laplacian operator, D^2 , for zonal wavenumber, m , is given by

$$D^2 = \frac{d^2}{dr^2} + \frac{1}{r} \frac{d}{dr} - \frac{m^2}{r^2}. \quad (10)$$

The $(D^2)^{-1}$ operator is the inverse of the D^2 operator and is given by the Green's function of D^2 . In order to define this Green's function we assume that the disk occupies the region $r_1 \leq r \leq r_2$, and at the boundaries we require that both the radial perturbation velocity and the perturbation vorticity vanish, i.e.,

$$\hat{u}(r_{1,2}, t) = \hat{\zeta}(r_{1,2}, t) = 0. \quad (11)$$

The perturbation vorticity is set to zero at the boundaries in order to avoid introduction of perturbation vorticity from the region outside the disk (the same boundary condition was introduced by Nolan & Farrell 1999 in the study of tornadogenesis). The interior boundary conditions do not influence the perturbation dynamics. Because of the large shear in the inner region, the perturbations rapidly develop high radial wavenumbers and are dissipated without being influenced by the boundary.

The perturbation evolution equation is rendered nondimensional by choosing a nondimensional time $\tilde{t} = \Omega_0 t$, nondimensional radial distance $\tilde{r} = r/r_0$, and nondimensional vorticity $\tilde{\zeta} = \hat{\zeta}/\Omega_0$. The nondimensional vorticity perturbation equation is

$$\frac{d\tilde{\zeta}}{d\tilde{t}} = -im\tilde{\Omega}(\tilde{r})\tilde{\zeta} - \tilde{U}(\tilde{r}) \frac{d\tilde{\zeta}}{d\tilde{r}} + i \frac{m}{2\tilde{r}} \frac{d\tilde{\Omega}(\tilde{r})}{d\tilde{r}} \tilde{D}^{-2} \tilde{\zeta} + \frac{1}{\text{Re}} \tilde{D}^2 \tilde{\zeta}, \quad (12)$$

where the tilde variables denote the nondimensional variables or operator, and the Reynolds number is defined as $\text{Re} = \Omega_0 r_0^2/\nu$. The nondimensional angular velocity is $\tilde{\Omega}(\tilde{r}) = \tilde{r}^{-3/2}$, and the nondimensional inflow is $\tilde{U}(\tilde{r}) = -3/(2\text{Re}\tilde{r})$. In the sequel we drop the tildes.

The nondimensional vorticity equation can be compactly written as

$$\frac{d\tilde{\zeta}}{d\tilde{t}} = \mathcal{A} \tilde{\zeta}, \quad (13)$$

where

$$\mathcal{A} = im\Omega \left[-1 - \frac{3}{4r^2} (D^2)^{-1} \right] - U \frac{d}{dr} + \frac{1}{\text{Re}} D^2. \quad (14)$$

The differential operators are discretized, and the evolution of the perturbation field is determined by forward propagation of the initial vorticity field according to

$$\zeta(t) = \Phi(t)\zeta_0, \quad (15)$$

where ζ_0 is the initial vorticity field and the propagator $\Phi(t)$ is given by the matrix exponential $\Phi(t) = e^{At}$.

2.1. Perturbation Energetics

The total kinetic perturbation energy, E , of single harmonic perturbations is given in terms of the radial perturbation velocity field u and azimuthal velocity field v as

$$E = \int_{r_1}^{r_2} \left(\frac{\overline{u^2}}{2} + \frac{\overline{v^2}}{2} \right) 2\pi\Sigma r dr, \quad (16)$$

where bars denote an average over an azimuthal wavelength of the real parts of the velocity components (i.e., $\overline{u^2} = \frac{1}{2}uu^*$). On integration by parts the kinetic energy can be expressed in terms of the stream function and vorticity as

$$E = -\frac{1}{2} \int_{r_1}^{r_2} \overline{\psi\zeta} 2\pi\Sigma r dr, \quad (17)$$

where now $\overline{\psi\zeta} = \frac{1}{4}(\psi^*\zeta + \zeta^*\psi)$. In terms of the discretized values of the vorticity field on a radial grid of size δ the perturbation energy can be also written as

$$E = \zeta^\dagger M \zeta, \quad (18)$$

where ζ is the column vector of the vorticity field values at the grid points, and the energy metric M is defined as the positive definite Hermitian matrix

$$M = -\frac{\pi\delta\Sigma}{4} \{ [(D^{-2})^{-1}]^\dagger R + R D^{-2} \}. \quad (19)$$

Here $(D^2)^{-1}$ is the matrix representation of the continuous operator $(D^2)^{-1}$, $[(D^2)^{-1}]^\dagger$ its Hermitian transpose, and R the diagonal matrix formed from the column vector of radial positions. We note that if we define the generalized velocity coordinate

$$z = \sqrt{M} \zeta, \quad (20)$$

the expression for the perturbation energy (18) can be recast as an ordinary Euclidean inner product in the new variable z :

$$E = z^\dagger z \equiv (z, z). \quad (21)$$

The nonlinearly valid energy tendency equation obtained from the field equations is

$$\begin{aligned} \frac{dE}{dt} = & - \int_{r_1}^{r_2} \left[r \frac{d\Omega(r)}{dr} \right] \overline{uv} 2\pi\Sigma r dr \\ & - \int_{r_1}^{r_2} \left(\overline{u^2} \frac{dU}{dr} + \overline{v^2} \frac{U}{r} \right) 2\pi\Sigma r dr \\ & - v \int_{r_1}^{r_2} \overline{|\nabla u|^2 + |\nabla v|^2} 2\pi\Sigma r dr. \end{aligned} \quad (22)$$

The first term of the energy tendency represents the rate of energy extraction from the mean flow. Because for Keplerian flow $d\Omega(r)/dr < 0$ this term leads to perturbation energy growth when the perturbation fields have velocity components such that $\overline{uv} > 0$, i.e., energy extracted from the

mean flow is fed to the perturbation field when the eddy angular momentum is directed outward. The second term is the energetic interaction of the inflow velocity with the perturbations. This term, which is negligible for typical astrophysical Reynolds numbers, contributes to perturbation growth when the rms perturbation azimuthal velocity field fluctuations exceed the corresponding fluctuations in the radial velocity field. The last term is the energy dissipation which is always a sink. Note that during periods of perturbation growth, angular momentum is invariably transferred outward if the inflow is negligible.

2.2. Generalized Stability Analysis of Nonnormal Systems

Traditionally, the stability of the mean flow is determined by eigenanalysis of the dynamical operator A that governs the linear perturbation dynamics. According to standard linear stability analysis, if all the eigenvalues (the spectrum) of the governing operator A are decaying (i.e., the real part of the eigenvalues is negative), the perturbations will decay at large times, at a rate equal to the maximum real part of the eigenvalues, and this is usually taken to indicate the stability of the mean flow.

However, there are many flows that are asymptotically stable but exhibit high transient growth, and the asymptotic estimates obtained from eigenanalysis of the governing operator are not indicative of the growth potential of perturbations in the flow. The asymptotic estimate is not indicative of the growth potential of perturbations when the governing operator is nonnormal in some physically pertinent inner product, which is usually taken to be the energy. A normal operator is one for which the commutator $AA^\dagger - A^\dagger A$ vanishes (A^\dagger is the adjoint operator or if the operator has been represented by a finite dimensional matrix A^\dagger is the Hermitian transpose), has orthogonal eigenvectors, and its stability is fully determined by the growth rate of the maximally growing eigenvalue of A . A nonnormal operator is one for which the commutator $AA^\dagger - A^\dagger A \neq 0$, the eigenvectors are nonorthogonal, and the growth potential of perturbations is obtained with the methods of generalized stability analysis (Farrell & Ioannou 1996, 1999a).

The operator governing the growth of perturbations in an astrophysical disk is nonnormal, and in order to assess the growth of perturbations in such a flow, we will apply the methods of generalized stability analysis.

In generalized stability analysis, the central object of study is the matrix propagator of the discretized linear perturbation equations, that is, the matrix that advances an initial state to a state of the system t units of time later. We choose to describe the system in generalized velocity coordinates z (cf. eq. [20]), and the propagator in these coordinates is given by the matrix $\Phi(t) = e^{Bt}$ where the matrix

$$B = M^{1/2} A M^{-1/2}, \quad (23)$$

governs the perturbation evolution in generalized velocity coordinates z :

$$\frac{dz}{dt} = Bz, \quad (24)$$

obtained by transforming equation (13) to generalized velocities.

The maximum energy growth that can be achieved at time t is given by the square of the spectral norm of the

propagator $||\Phi(t)||^2$, which is found from the singular value decomposition

$$\Phi(t) = U\Sigma V^\dagger. \tag{25}$$

Matrices U and V are unitary, and Σ is diagonal with positive elements. The diagonal elements σ_i of Σ give the square root of the energy growth at time t of the initial perturbation specified by the corresponding column of V . The elements of σ_i are ordered decreasing in magnitude. The matrix V provides a convenient orthogonal decomposition of the perturbation state space in which each element of the space is identified by the growth it produces in time t . Each element of this space is mapped at time t to the corresponding column of U amplified by the corresponding element of the diagonal matrix Σ . In this way we characterize all the perturbations according to their growth potential and determine the perturbation subspace that produces perturbation growth. The perturbation that leads to the largest growth in time t is given by the first column of V , and the energy growth produced by this perturbation is σ_1^2 . This perturbation is called the optimal perturbation and its associated growth, σ_1 , the optimal growth (Farrell 1988). The spectral norm of the propagator at time t is defined to be the optimal growth, i.e., $||\Phi(t)|| = \sigma_1$. The aim of generalized stability analysis is to calculate the optimal growth in the flow for all times and identify the optimal perturbations that produce it.

3. GENERALIZED STABILITY ANALYSIS OF KEPLERIAN DISKS

We illustrate the response of Keplerian disks by calculating the energy growth of optimal perturbations. For definiteness we choose the disk to have an inner radius of $r_1 = 0.1r_0$ and outer radius of $r_2 = 5r_0$. The qualitative character of the results presented in the sequel do not depend on the size of the disk.

The Keplerian disk is stable at all wavenumbers and Reynolds numbers. The maximum growth rate associated with the least damped eigenmode of the evolution operator \mathcal{A} is plotted in Figure 1 (*top left panel*) as a function of zonal wavenumber m for various Reynolds numbers. For Reynolds number $Re = 10^3$ and zonal wavenumber $m = 1$, the e -folding time is about 100 nondimensional time units or about 15 rotational periods of the disk (evaluated at radius $r = r_0$). In the same figure (*top right panel*) we calculate the corresponding maximum optimal energy growth factors that can be achieved as a function of zonal wavenumber and for Reynolds numbers ranging between $Re = 10^3$ and 10^6 . For zonal wavenumber $m = 1$ and Reynolds number $Re = 10^3$ the maximum optimal energy growth factor is about 80, despite the asymptotic stability of the linearized operator. The optimal energy growth factor as a function of time, measured in rotational periods, for Reynolds number $Re = 10^4$ and zonal wavenumbers $m = 1, 2, 3$ are shown in Figure 1 (*bottom left panel*). Because of their higher growth,

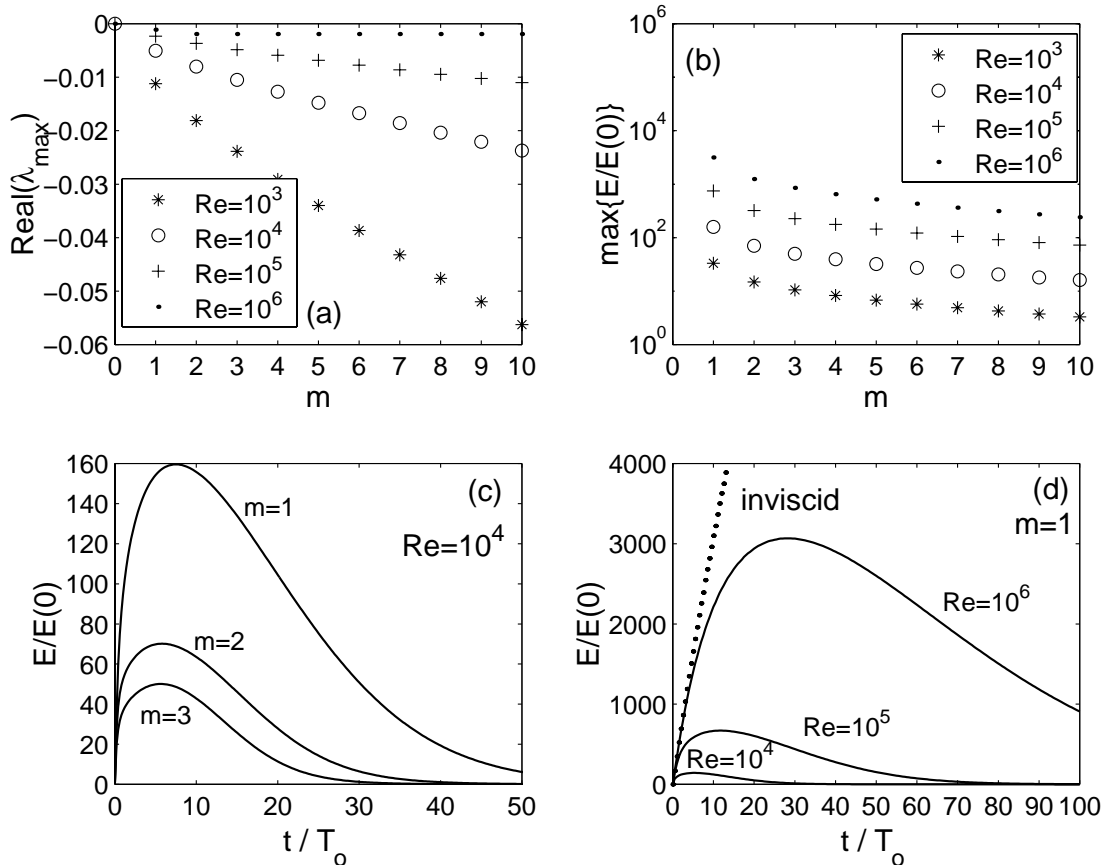


FIG. 1.—(a) Growth rate of the least damped mode of operator \mathcal{A} as a function of zonal wavenumber m for several Reynolds numbers for a Keplerian disk extending between $r_1 = 0.1r_0$ and $r_2 = 5r_0$. The disk is asymptotically stable. (b) For the same disk the maximum energy perturbation growth factor that can be achieved as function of zonal wavenumber m for various Reynolds numbers. (c) The optimal energy growth factor as a function of time measured in rotational periods (T_0) for zonal wavenumbers $m = 1, 2, 3$ at Reynolds number $Re = 10^4$. The $m = 1$ perturbations dominate the perturbation dynamics. (d) Optimal energy growth factor as a function of time for $m = 1$ and several Reynolds numbers.

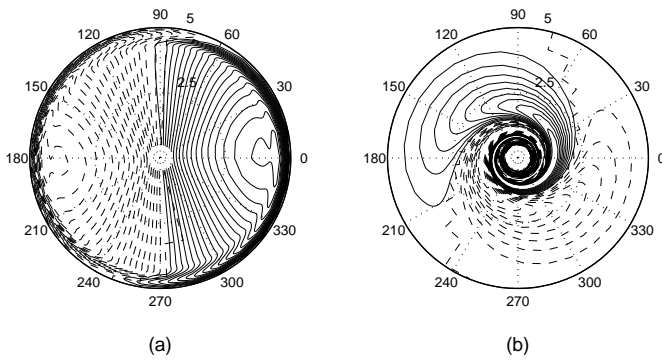


FIG. 2.—(a) Stream function of the least damped mode for a Keplerian disk extending from $r_1 = 0.1r_0$ to $r_2 = 5r_0$ for zonal wavenumber $m = 1$ and Reynolds number $Re = 10^4$. The e -folding time is about 32 rotational periods (T_0) at r_0 . (b) The stream function of the optimal perturbation with $m = 1$ that maximizes the energy growth factor in one rotational period in the same Keplerian disk. The energy growth factor at one rotational period is 95. The optimal perturbation leads, leaning against the shear, in order to grow.

zonal wavenumber $m = 1$ perturbations are expected to dominate the perturbation field. The energy grows rapidly, and even in one period substantial energy perturbation growth is achieved. The maximum optimal growth factor (top right panel) for $m = 1$ and Reynolds number $Re = 10^4$

is 160 and occurs at about $8T_0$ (T_0 denotes a rotational period of the disk at radius r_0). The optimal energy growth factor increases with Reynolds number (bottom right panel), because with reduced dissipation the perturbations can lean more against the shear without being dissipated and in this way achieve higher energy growth factors at the optimizing time. The inviscid perturbation growth is also shown at the bottom right panel of Figure 1.

The eigenmodes of the disk bear no resemblance to the optimal perturbations. For example, the stream function of the least damped mode for zonal wavenumber $m = 1$ and Reynolds number $Re = 10^4$ is shown in Figure 2a. It is concentrated in the outer region of the disk where the mean shear is small and the mode can decay with the least damping. Moreover, the momentum flux associated with the least damped mode yields no tendency for mass accretion, as $\overline{wv} < 0$ at all radii. The stream function of the optimal perturbation of the same flow that grows by a factor of 95 in energy in a single period is shown in the right panel of Figure 2. The optimal perturbation is leading, leaning against the shear in order to produce the required positive angular momentum transfer which is necessary for energy growth according to the energetic requirements (cf. eq. [22]). The optimal perturbation is also concentrated near the radius r_0 in order to take advantage of the large value of the shear at this location. The optimal perturbation

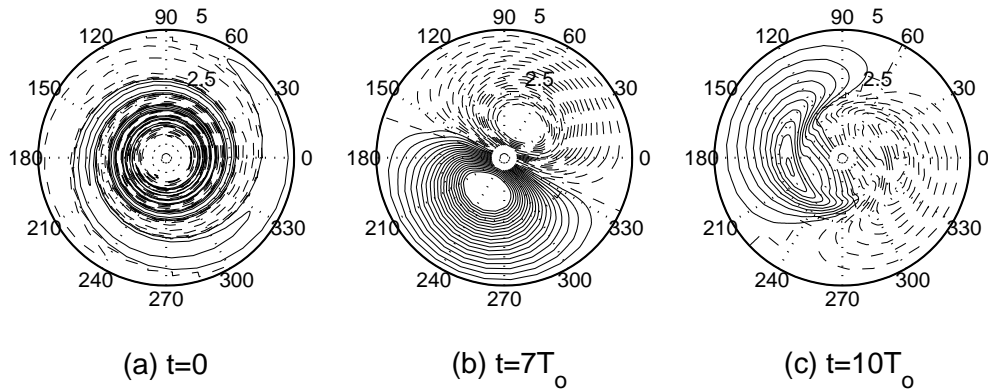


FIG. 3.—(a) Stream function at $t = 0$ of the $m = 1$ optimal perturbation that maximizes the energy growth factor at $t = 7T_0$ ($T_0 =$ one rotational period). The perturbation has initially unit energy. The Keplerian disk extends from $r_1 = 0.1r_0$ to $r_2 = 5r_0$, and the Reynolds number is $Re = 10^4$. The perturbation leads. (b) The optimal perturbation at $t = 7T_0$ (the optimizing time). The energy of the perturbation is 159. (c) The optimal perturbation at $t = 10T_0$. The perturbation trails and the perturbation energy is decaying. The energy of the perturbation at this time is 10.

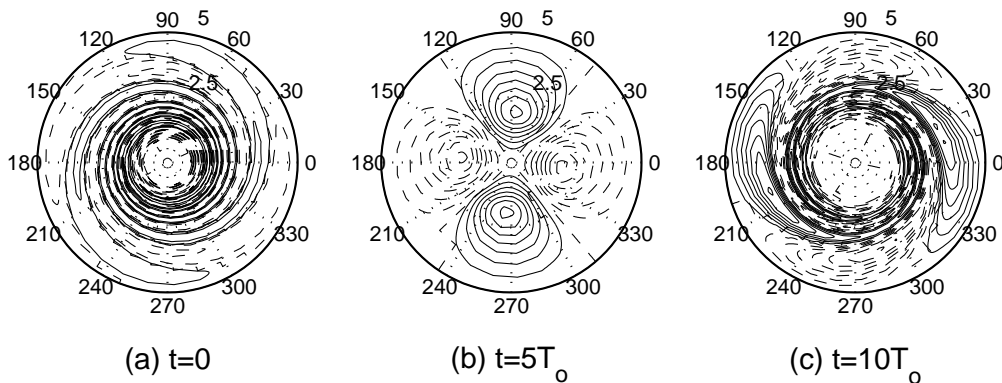


FIG. 4.—(a) Stream function at $t = 0$ of the $m = 2$ optimal perturbation (of unit energy) that maximizes the energy growth factor in $5T_0$. The Keplerian disk extends from $r_1 = 0.1r_0$ to $r_2 = 5r_0$, and the Reynolds number is $Re = 10^4$. The perturbation leads. (b) The optimal perturbation at $t = 5T_0$ (the optimizing time). The energy of the perturbation at this time is 70. (c) The optimal perturbation at $t = 10T_0$. The perturbation trails and the perturbation energy is decaying. The energy of the perturbation at this time is 0.53.

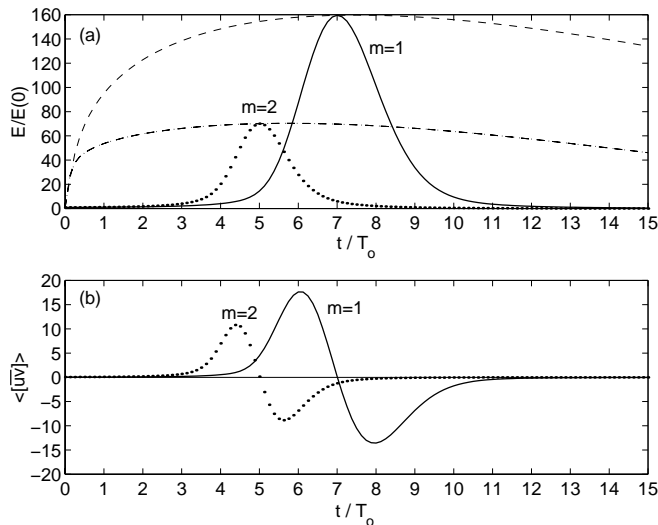


FIG. 5.—(a) Evolution of the energy of the $m = 1$ optimal perturbation that maximizes the energy growth factor at $t = 7T_0$ and evolution of the energy of the $m = 2$ optimal perturbation that maximizes the energy growth factor at $t = 5T_0$. Time is measured in rotational periods (T_0). The disk is Keplerian and extends from $r_1 = 0.1r_0$ to $r_2 = 5r_0$, and the Reynolds number is $Re = 10^4$. The dashed lines are the optimal energy growth factor for perturbations of zonal wavenumber $m = 1$ and $m = 2$ as a function of optimizing time. (b) The corresponding total angular momentum transfer per unit mass of the same optimal perturbations as a function of time (in rotational periods). The total angular momentum transfer per unit mass is defined as $\langle [uv] \rangle$, where $[·]$ denotes a radial average, and the bar denotes a zonal average.

at $t \rightarrow \infty$ becomes the least damped mode but with a greatly amplified magnitude.

The evolution of the optimal perturbation with zonal wavenumber $m = 1$ that produces optimal energy growth factor at $t = 7T_0$ is shown in Figure 3. The perturbation is shown at the initial time $t = 0$, the optimizing time $t = 7T_0$ and at $t = 10T_0$. The optimal perturbation as discussed earlier is initially leading, its stream function contours

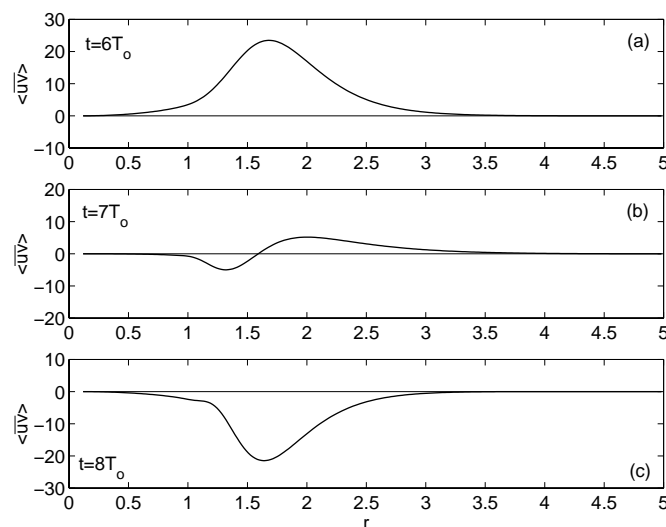


FIG. 6.—Radial distribution of the momentum flux associated with the $m = 1$ optimal perturbation that maximizes the energy growth factor at $t = 7T_0$. The disk is Keplerian and extends from $r_1 = 0.1r_0$ to $r_2 = 5r_0$, and the Reynolds number is $Re = 10^4$. (a) The momentum flux at $t = 6T_0$. The momentum flux is everywhere outward. (b) The momentum flux at $t = 7T_0$, the optimizing time. (c) The momentum flux at $t = 8T_0$. The momentum flux is everywhere inward.

leaning against the shear, in order to grow. The phase lines of the stream function rotate with time in the direction of the shear. For example, at the optimizing time the phase lines are aligned with the mean shear and at $t = 10T_0$ the perturbation trails. Eventually, the perturbation will assume the form of the least damped mode (Fig. 2a). The energy evolution of this optimal perturbation is shown in Figure 5a. Similar is the evolution of higher wavenumber optimals. In Figure 4 the evolution of the $m = 2$ optimal that optimizes energy growth factor in $t = 5T_0$ is shown. The corresponding energy evolution of this perturbation is shown in Figure 5a. All growing perturbations share these characteristic patterns during their growth and decay period. This is dictated by the energy tendency equation and has been described in the astrophysical literature in the pioneering work of Goldreich & Lynden-Bell (1965) and Toomre (1964, 1981). The energy tendency equation (22) requires that during the growing phase angular momentum is transported outward (shown in Fig. 6a), and during the decay phase there must be inward transport of angular momentum (shown in Fig. 6c). The evolution of the angular momentum flux averaged over the whole disk is shown for the selected zonal $m = 1$ and $m = 2$ optimal perturbations in Figure 5b. Averaged over their life cycle the angular momentum transport by these perturbations is found to be positive. We shall show in the sequel that when a full spectrum of perturbations is imposed on the disk the angular momentum transport is robustly outward.

4. PERTURBATION STRUCTURE UNDER STOCHASTIC FORCING

We have demonstrated that Keplerian disks despite their asymptotic stability support strong transient growth of a subset of perturbations which during their growth phase transport angular momentum outward. In order to demonstrate the plausibility of the hypothesis that mass accretion in disks emerges naturally in Keplerian disks in the presence of background perturbation, we demonstrate that a mean outward angular momentum transfer will invariably result when the disk is stochastically forced; and in order to demonstrate the inherent dynamical role of the disk differential rotation in organizing the perturbation structure to produce mean outward momentum flux, we consider noise sources which are white in time and space.

Because the disk is asymptotically stable, it will reach a statistically steady state when subjected to continual stationary stochastic forcing. The forcing may be due to external processes, or it may be considered as a parameterization of the neglected nonlinear terms. Possible sources of forcing are tidal interaction in binaries, outbursts in binary systems, or perturbation debris from shock waves. If the disk is in a turbulent state, the stochastic forcing may represent a parameterization of the backscattering due to the neglected nonlinear terms in the dynamics (DeSole 1996, 1999). In that sense the stochastically forced model of a Keplerian disk provides a model of the energy bearing scales of the turbulent disk. Such a parameterization has been very successful in modeling the perturbation variance in other shear flows (Farrell & Ioannou 1993a, 1993c, 1995, 1998, 1999b). Owing to the nonnormality of the operator governing the dynamics, the structure, and color of the forcing is essentially inconsequential because the response of the disk will be dominated by the strongly growing transient structures, and as long as the forcing projects on these its detailed color

is unimportant. It has been demonstrated in other studies that this is the case (Farrell & Ioannou 1994, 1995, 1999b). In this section we will consider that the whole disk is forced at all scales and at all frequencies. The effects of spatial and temporal localization of the forcing on the angular momentum transfer will be discussed in the next section.

We incorporate in the perturbation dynamics the forcing term $F\eta(t)$, where $\eta(t)$ is temporally Gaussian white noise which is spatially δ -correlated with zero ensemble mean and unit ensemble covariance, i.e.,

$$\langle \eta_j(t) \rangle = 0, \quad \langle \eta_i(t_1) \eta_j^*(t_2) \rangle = \delta_{ij} \delta(t_1 - t_2), \quad (26)$$

and F is a matrix specifying the radial structure of the forcing, $\langle \cdot \rangle$ denotes an ensemble average. In this section we will assume that F is unitary, i.e., $F^\dagger F = I$, where I is the identity. Under unitary stochastic forcing the same amount of energy is imparted to all radial scales in the disk. The generalized velocity perturbation fields satisfy the following equation:

$$\frac{dz}{dt} = Bz + F\eta(t), \quad (27)$$

where $B = M^{1/2}AM^{-1/2}$ as in equation (23).

The dynamical operator A is stable, and, consequently, the forced Keplerian disk will reach a statistical steady state with finite variance. The statistical steady state will be characterized by a correlation matrix $C = \langle zz^\dagger \rangle$, which can be obtained (Farrell & Ioannou 1999b) from the forced solution of equation (27):

$$z(t) = \int_0^t e^{B(t-s)} F \eta(s) ds. \quad (28)$$

The correlation matrix at time t can then be calculated utilizing the properties of the white noise forcing (eq. [27]):

$$\begin{aligned} C_{ij}(t) &= \langle z_i(t) z_j^*(t) \rangle \\ &= \left[\left\langle \int_0^t ds \int_0^t ds' e^{B(t-s)} F \eta(s) \eta^\dagger(s') F^\dagger e^{B^\dagger(t-s')} \right\rangle \right]_{ij} \\ &= \left[\int_0^t e^{B(t-s)} F F^\dagger e^{B^\dagger(t-s)} ds \right]_{ij}. \end{aligned} \quad (29)$$

The ensemble average perturbation total energy $\langle E(t) \rangle$ accumulated at time t is then the trace of the correlation matrix $C(t)$, which in dimensional units is given by

$$\langle E(t) \rangle = \frac{\dot{E}_{in}}{\Omega_0} \text{trace} [C(t)], \quad (30)$$

where \dot{E}_{in} is the total energy input rate (ergs s^{-1}) by the random forcing and Ω_0 the rate of rotation of the disk at r_0 .

We can obtain the correlation matrix of the statistical steady state by noting that differentiation of equation (29) leads to a differential equation for the time rate of change of the correlation matrix:

$$\frac{dC(t)}{dt} = FF^\dagger + BC(t) + C(t)B^\dagger. \quad (31)$$

Because of the asymptotic stability of the Keplerian disk, the time rate of change of the correlation matrix tends to zero as $t \rightarrow \infty$, and therefore the asymptotic correlation matrix that describes the statistical steady state, C^∞ , must

satisfy the algebraic Lyapunov equation:

$$BC^\infty + C^\infty B^\dagger = -FF^\dagger, \quad (32)$$

which can be readily solved to obtain the correlation matrix C^∞ that determines the statistically steady state. Note that when all the degrees of freedom are forced with unitary forcing structures that satisfy $FF^\dagger = I$, the asymptotic correlation matrix does not depend of the specific choice of the elements of the forcing matrix F .

The perturbation structure under stochastic forcing is revealed by the empirical orthogonal functions (EOFs), which are the orthogonal eigenfunctions of the correlation matrix. Each eigenvalue of the positive definite Hermitian correlation matrix C^∞ equals the energy accounted for, under unbiased forcing, by the pattern of its corresponding eigenvector, and the pattern that corresponds to the largest eigenvalue contributes most to the perturbation energy at the statistical steady state. Note that because of the non-normality of A , the eigenfunctions of the correlation matrix, the EOFs, are distinct from the eigenfunctions of A . The dominant zonal wavenumber $m = 1$ and $m = 2$ patterns that emerge in the stochastically forced disk with unitary forcing are shown in Figure 7. These top EOFs are similar to the structure of the optimal perturbations at their peak energy as can be seen by comparing with the structures in the middle panels of Figure 3 and Figure 4. The top EOFs account, respectively, for about 70% and 50% of the maintained energy in the statistical steady state, and as it can be seen in Figure 7 only the first five EOFs are needed in order to span the total perturbation field energy. The maintained variance for $m = 1$ perturbations is 3 times larger than the energy maintained by the $m = 2$ mode under stochastic forcing of equal magnitude, and the momentum transfer associated with $m = 1$ perturbations is 1 order of magnitude larger than that due to the $m = 2$ mode. The perturbation dynamics are therefore expected to be dominated by zonal $m = 1$ perturbations.

The correlation matrix determines all the quadratic Reynolds stresses associated with the statistical equilibrium. For if we are interested in evaluating the matrix $G_{ij} = \langle f_i g_j^* \rangle$ for fields f and g that are dependent linearly on the generalized velocity z , i.e., for $f = Tz$ and $g = Sz$, then the correlation matrix G can be expressed in terms of C^∞ as $G = TC^\infty S^\dagger$. The quantity of interest is the correlation matrix of the radial and zonal velocity, from which the angular momentum flux distribution can be derived. This correlation matrix is

$$C_{ij}^{uv} = \overline{\langle (u_i e^{im\theta})(v_j e^{im\theta})^* \rangle},$$

where u_i is the amplitude of the radial velocity at $r = r_i$ and v_j the amplitude of the zonal velocity at $r = r_j$; the bar denotes a zonal average. The correlation matrix can be equivalently written as $C_{ij}^{uv} = \frac{1}{2} \Re \langle u_i v_j^* \rangle$ where \Re denotes the real part of a complex quantity. The amplitude of the radial velocity u for a perturbation of zonal wavenumber m is given in terms of the generalized velocity z by $u = -imR^{-1}M^{-1/2}z$, while the amplitude of the zonal velocity is given by $v = DM^{-1/2}z$, where D is the matrix representation of the differential operator d/dr . Therefore,

$$C^{uv} = \frac{1}{2} \Re \langle uv^* \rangle = \frac{m}{2} R^{-1} M^{-1/2} \Im(C^\infty) M^{-1/2} D^\dagger, \quad (33)$$

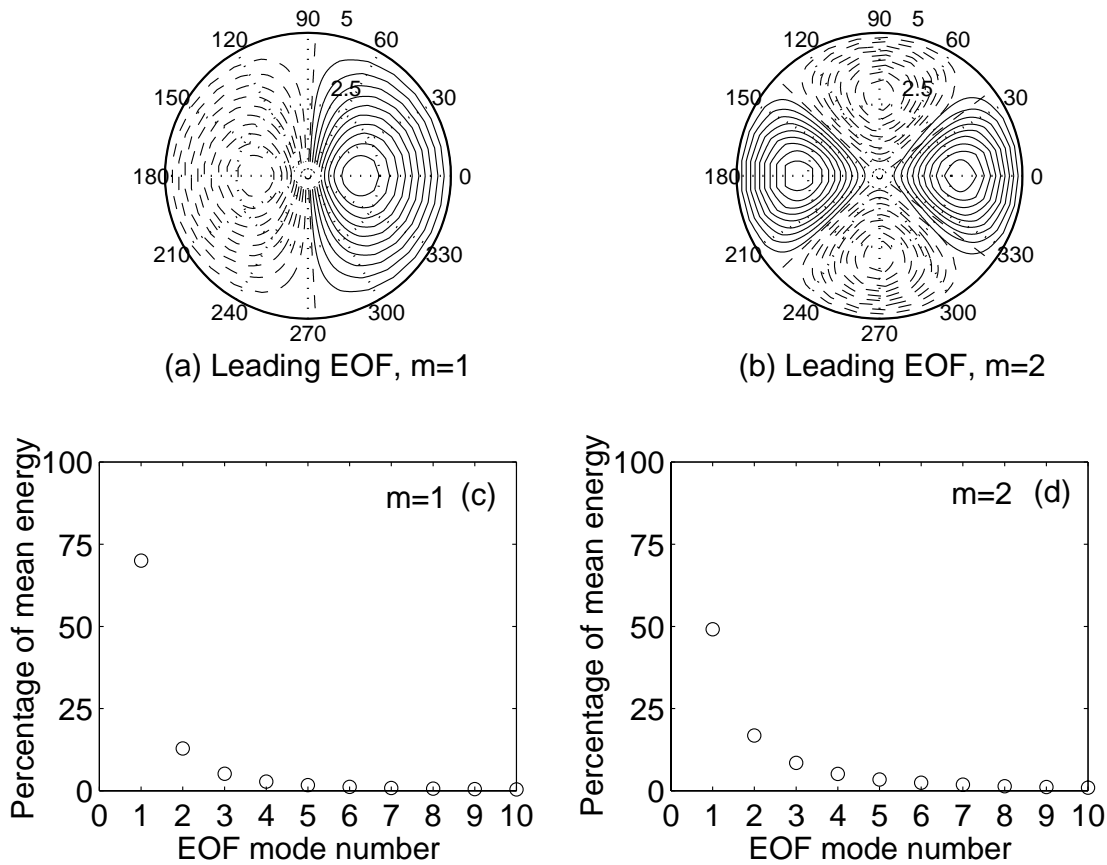


FIG. 7.—(a) Stream function of the first EOF for zonal $m = 1$ perturbations. This empirical function accounts for 70% of the mean energy. (b) The corresponding stream function of the first EOF for zonal $m = 2$ perturbations. This EOF accounts for 50% of the mean energy. (c) Percentage ensemble mean energy accounted for by the first 10 EOFs of the velocity correlation matrix ordered according to their contribution to the ensemble mean. The case shown is for $m = 1$ perturbations. Note that 90% of the ensemble mean energy is accounted for by the first 5 EOFs. (d) The same as in (c) but for $m = 2$ perturbations. In this case the first 10 EOFs account for 90% of the ensemble mean energy. The disk is Keplerian and extends from $r_1 = 0.1r_0$ to $r_2 = 5r_0$; the Reynolds number is $\text{Re} = 10^4$.

where $\Im(C^\infty)$ denotes the imaginary part of the correlation matrix. The diagonal elements of C^{uv} , denoted $\text{diag}(C^{uv})$, determine the radial distribution of the ensemble averaged eddy angular momentum flux. In dimensional units the radial distribution of the mean angular momentum flux per unit mass is given by

$$\langle \overline{uw} \rangle = \frac{\dot{E}_{\text{in}}}{2\pi\Sigma r_0^2 \Omega_0} \text{diag} \left(\frac{m}{2} \mathbf{R}^{-1} \mathbf{M}^{-1/2} \Im(C^\infty) \mathbf{M}^{-1/2} \mathbf{D}^\dagger \right). \quad (34)$$

The radial distribution of the momentum flux derived in equation (34) for the case of unitary forcing, i.e., for forcing that satisfies $\mathbf{F}\mathbf{F}^\dagger = \mathbf{I}$, will be compared to the flux obtained by demanding constancy of the mean angular momentum flux across a disk in equilibrium under the assumption that the viscous contribution to the mean angular momentum balance is negligible (Shakura & Sunyaev 1973; Pringle 1981; Balbus & Hawley 1998; Balbus & Papaloizou 1999):

$$\langle \overline{uw} \rangle = \frac{\dot{M}\Omega(r)}{2\pi\Sigma} \left(1 - \sqrt{\frac{R_0}{r}} \right), \quad (35)$$

where \dot{M} is the equilibrium constant accretion rate and R_0 is the radius at the inner boundary of the disk. There is no reason for the radial distribution predicted by equation (34), for an appropriately chosen energy input \dot{E}_{in} , to be the same

with the angular momentum flux distribution predicted by equilibrium theory. If they are, it suggests that the equilibrium angular momentum distribution (35) arises as the first-order effect of stochastically forcing a viscous disk, in which the Reynolds number is based on an appropriate eddy viscosity. It further suggests that the energy-bearing perturbation structure in Keplerian disks is organized by the linear shear dynamics and that the effects of the nonlinear terms in the turbulent disk can be parameterized by added diffusion and stochastic forcing. Similar conclusions have been reached for shear turbulence in other settings (Farrell & Ioannou 1993a, 1995, 1998; DelSole 1996, 1999). The equilibrium and the stochastically induced angular momentum distribution for zonal wavenumbers $m = 1$ and $m = 2$ are compared in Figure 8. The comparison is made for $\text{Re} = 10^4$, but the distribution does not vary appreciably with Reynolds number. The agreement between the two curves is good, especially for the dominant $m = 1$ structures. It is to be noted that the deduced angular momentum fluxes are everywhere outward, implying that in the absence of any instabilities the natural response of a stochastically forced Keplerian disk is to accrete mass. It also suggests that the eddy fields in an accretion disk may be approximately nondivergent.

Matching the maxima of the two angular momentum flux distributions provides a relationship between the energy input by the stochastic forcing and the resulting mass accre-

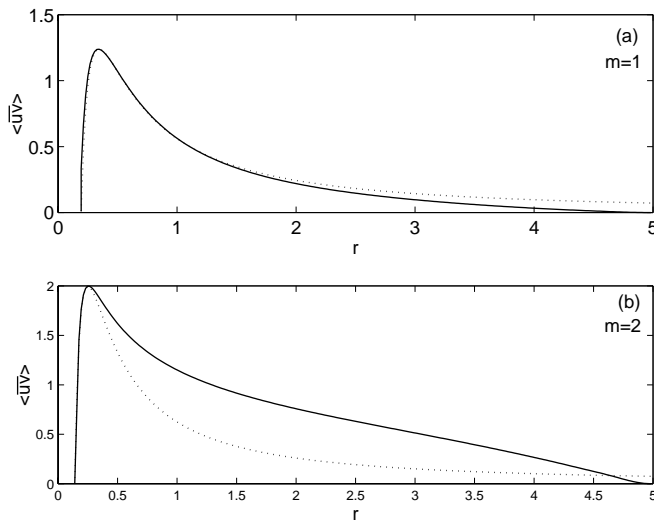


FIG. 8.—(a) Radial distribution of the momentum flux sustained by the dominant $m = 1$ perturbations in the statistically steady state. The dotted line is the equilibrium theory momentum flux given by eq. [35]. (b) Same as (a), but for $m = 2$ perturbations. Under the same forcing the fluxes of the $m = 2$ perturbations are 1 order of magnitude smaller than those of the $m = 1$ perturbations. The disk is Keplerian and extends from $r_1 = 0.1r_0$ to $r_2 = 5r_0$; the Reynolds number is $\text{Re} = 10^4$.

tion rate. This relation enables us to estimate the stochastic energy input required to produce observed levels of mass accretion. The accretion rate will be estimated from the observed accretion luminosity which is related to the accretion rate \dot{M} by $L_{\text{acc}} = GM\dot{M}/R_*$, where R_* is the radius of the central body and M its mass. If the disk is externally forced, we expect $L_{\text{acc}} > \dot{E}_{\text{in}}$. On the other hand, if the disk is in a turbulent state and \dot{E}_{in} parameterizes the energy transfer to the energy bearing $m = 1$ scale from smaller scales by the nonlinear terms, then energy flux between scales in the turbulent energy cascade demands, for balance in the steady state, only that $\dot{E}_{\text{out}} - \dot{E}_{\text{in}} = \dot{D}$, where \dot{E}_{out} is the energy that is transferred from the $m = 1$ perturbations to the smaller scales, and \dot{D} is the rate of dissipation (which exceeds L_{acc}) and the magnitude of \dot{E}_{in} is undetermined. In fact, if we determine that the energy input is comparable to L_{acc} , this is an indication that the disk must be turbulent and the anomalous viscosity is being created by the turbulent stresses. Alternatively, if observation shows that $L_{\text{acc}} \gg \dot{E}_{\text{in}}$, then, while the possibility that the disk is turbulent cannot be excluded, accretion could result from pure external forcing.

The energy input is related to the mass accretion rate by

$$\dot{E}_{\text{in}} = 0.1f(\text{Re}, m) \frac{r_0^{7/2}}{R_0^{3/2}} \Omega_0^2 \dot{M}, \quad (36)$$

where the nondimensional function $f(\text{Re}, m)$ is defined as

$$\frac{1}{f(\text{Re}, m)} = \max \left\{ \text{diag} \left[\frac{m}{2} \mathbf{R}^{-1} \mathbf{M}^{-1/2} \mathfrak{I}(\mathbf{C}^\infty) \mathbf{M}^{-1/2} \mathbf{D}^\dagger \right] \right\}. \quad (37)$$

Because of the dominance of the zonal wavenumber $m = 1$ perturbations, we determine the behavior of $f(\text{Re}, m)$ for $m = 1$ as a function of Reynolds number, “Re.” We find that $f(\text{Re}, 1)$ is nearly independent of Reynolds number and that it assumes the value $f(\text{Re}, 1) \simeq 0.2$. Consequently, the

ratio between the energy input required to produce accretion \dot{M} and the corresponding luminosity L_{acc} for that accretion rate becomes for large Reynolds numbers:

$$\frac{\dot{E}_{\text{in}}}{L_{\text{acc}}} = 0.02 \sqrt{\frac{r_0}{R_*}}, \quad (38)$$

where the inner boundary of the disk is taken at the stellar surface, $R_0 = R_*$. This expression indicates that the energy input needed to maintain a given accretion of mass is proportional to the square root of the radial size of the disk. For accretion disks around the active galactic nuclei (AGN) the accretion luminosity is given by $L_{\text{acc}} = \eta \dot{M} c^2$, where η is a radiation efficiency and c the speed of light (Frank, King, & Raine 1992), and if the inner radius of the disk is taken to be the Schwarzschild radius, $R_* = 2GM/c^2$, we obtain

$$\frac{\dot{E}_{\text{in}}}{L_{\text{acc}}} = \frac{7 \times 10^{-3}}{\eta} \frac{c}{r_0 \Omega_0}. \quad (39)$$

Ratios (38) and (39) are estimated for astrophysical disks with parameters given in Table 1. For binary systems we consider the case of dwarf novae, for AGNs the case of the mildly active galaxy NGC 4258 (Lin & Papaloizou 1996), and for young stellar objects (YSOs) we consider the inner part of HL Tau disk system (Sargent & Beckwith 1991; Ohashi & Hayashi 1996; Lin & Papaloizou 1996).¹ If we assume that the forcing structures, F , are unitary, the required energy input to maintain the observed accretion luminosity is found to be $\dot{E}_{\text{in}}/L_{\text{acc}} \simeq 0.1$ for binary systems, $\dot{E}_{\text{in}}/L_{\text{acc}} \simeq 2.8$ for YSOs, and $\dot{E}_{\text{in}}/L_{\text{acc}} \simeq 5 \times 10^3$ for AGNs. Therefore, observed levels of accretion could result by spatially white external forcing in binary systems and possibly for YSOs, but AGN accretion disks are probably in a turbulent state and accretion ensues from the turbulent Reynolds stresses.

In the calculations above a mean inward radial velocity $U(r) = -3/(2\text{Re} r)$ was assumed for reasons of consistency, which for the nearly inviscid calculations presented above is negligible. The effect of a mean radial inflow on the stochastic equilibrium can be assessed by considering for all “Re” a mean inflow of the form: $U(r) = -3/(2 \times 10^4 r)$. The

¹ HL Tau is a very young object ($< 10^5$ yr) with a very large accretion rate and with its outer part free falling. It is probably in a transitional stage, and the inner Keplerian disk is fed by the surroundings. We use this example as an extreme case of YSO accretion, while T Tau stars have about 2 orders of magnitude lower accretion rates.

TABLE 1
PARAMETERS OF ASTROPHYSICAL ACCRETION DISKS

	Binary Systems (DN System)	YSO (HL Tau)	AGN (NGC 4258)
M_* (M_\odot)	1	0.5	4×10^6
R_0	10^7 m	$1 R_\odot$...
\dot{M} ($M_\odot \text{ yr}^{-1}$)	10^{-10}	5×10^{-6}	7×10^{-5}
M_{disk} (M_\odot)	10^{-11}	0.1	4×10^6
r_0	3×10^8 m	100 AU	10 pc
Efficiency η	0.01
L_{acc} (ergs s^{-1})	8×10^{32}	3×10^{35}	4×10^{40}
$\dot{E}_{\text{in}}/L_{\text{acc}}$	$0.56f(\text{Re}, m)$	$14.14f(\text{Re}, m)$	$2.52 \times 10^4 f(\text{Re}, m)$

NOTE.—Data from Sargent & Beckwith 1991; Ohashi & Hayashi 1996; Lin & Papaloizou 1996.

excess unbalanced inflow for $Re > 10^4$ is assumed here to outflow in a deformation region in the inner radius of the disk. In that case the stochastic forcing input required to produce a given value of mass accretion diminishes and it is found that, for $m = 1$, $f(Re, m)$ becomes asymptotically

$$f(Re, 1) \approx \frac{4000}{Re}. \quad (40)$$

An existing inflow can thus lead to a dramatic increase of the accretion rate. For the astrophysical disks considered and $Re = 10^{10}$ the previously calculated ratios become $\dot{E}_{in}/L_{acc} \simeq 2 \times 10^{-7}$ for binary systems, $\dot{E}_{in}/L_{acc} \simeq 5 \times 10^{-6}$ for YSOs, and $\dot{E}_{in}/L_{acc} \simeq 10^{-2}$ for AGNs, indicating that in all cases external forcing could maintain the accretion rate if it were spatially distributed and broadband.

5. EFFECT OF SPATIAL AND TEMPORAL LOCALIZATION OF THE FORCING

We have considered a disk that was stochastically forced with forcings distributed throughout the disk, and the forcing was assumed to be temporally and spatially white. In that case we find that the maintained perturbations flux angular momentum is outward supporting accretion of mass to the central body. However, if the forcing is spatially localized and is temporally and spatially band-limited, the resulting angular momentum flux will in general depend on the specific forcing. We here present an investigation of the effect of spatial and temporal localization of the forcing on the maintained angular momentum flux in statistical equilibrium.

In order to examine the effect of the structure and color of the forcing on the maintained equilibrium, we identify the forcing structures that are responsible for producing the variance. We can identify these forcing structures by forming the ensemble mean perturbation energy, $\langle E \rangle = \langle z^\dagger z \rangle$, which, by using equation (28) and the properties of the white noise given in equation (26), can be written conveniently as the quadratic form:

$$\langle E \rangle = \mathbf{F}^\dagger \mathbf{K} \mathbf{F}, \quad (41)$$

where \mathbf{F} denotes the matrix having as its columns the spatial structures of the forcing and the stochastic matrix \mathbf{K} , that defines the quadratic form, is given by

$$\mathbf{K} = \int_0^\infty e^{\mathbf{B}^\dagger s} e^{\mathbf{B} s} ds. \quad (42)$$

The eigenvectors of the Hermitian matrix \mathbf{K} determine an orthonormal set of forcings, which, when ordered in decreasing order of the magnitude of their eigenvalues, order the forcings according to contribution in producing the maintained perturbation energy. These forcing structures are called stochastic optimals (Farrell & Ioannou 1996, 1999b).

The first and 26th stochastic optimal for a Keplerian disk at Reynolds number $Re = 10^4$ is shown in Figure 9. The percentage of the variance produced by the stochastic optimals is also shown in the same graph. The first stochastic optimal, responsible for producing 23% of the variance, is distinct from the first EOF and the least damped mode of the system; this is a reflection of the nonnormality of the operator \mathbf{B} governing the perturbation dynamics. The first stochastic optimals are similar in structure to the optimal perturbations; they lean against the mean flow shear and,

consequently, when forced lead to angular momentum expulsion. Indeed, if we limit the stochastic forcing to include only the structures of the first 25 stochastic optimals, by choosing the columns of the forcing matrix \mathbf{F} to be the first 25 stochastic optimals, the maintained angular momentum flux is everywhere positive (except in a region at small radius). This is shown in Figure 10. If, on the other hand, the forcing is limited to the higher order stochastic optimals (e.g., by forcing only the stochastic optimals of order greater than the 25th) then the angular momentum transfer is everywhere negative, implying an outward mass transfer. But, as shown in Figure 10, the net positive angular momentum flux produced by forcing with the first stochastic optimals is not canceled by the negative angular momentum flux produced by forcing with the stochastic optimals of higher order, and the sum of the two angular momentum fluxes is equal to the net outward angular momentum flux produced by the union of these forcings. This incomplete cancellation of the angular momentum fluxes can be traced to the lack of symmetry in the angular momentum fluxes produced during the growth and decay phases of the evolution of perturbations. During their growth phase, perturbations flux angular momentum outward, as is required by the energy tendency equation (22), while during their decay phase, they flux angular momentum inward (cf. Fig. 6). The upgradient and downgradient fluxes associated with the growth and decay phase would cancel in the absence of dissipation and in the absence of analytic modes in the disk, which act as a repository of the energy extracted from the flow during perturbation growth and destroy the structural symmetry between the growth and decay phases. Complete reversibility in the angular momentum fluxes occurs, for example, in the idealized situation of an unbounded constant shear flow (Farrell & Ioannou 1993b), in which case there are no analytic modes. The presence of modes breaks the symmetry between growth and decay phases with the energy extracted from the mean flow during the growing phase being transferred to the modal structures which do not shear over and, hence, do not transfer all the angular momentum flux accumulated during perturbation growth back to the mean flow (Farrell & Ioannou 1993b).

The sign of the angular momentum flux depends on the degree of projection of the specific stochastic forcing on the stochastic optimals. If the stochastic forcing excites all the stochastic optimals equally, as is the case of unitary forcing presented earlier, the angular momentum flux is positive. If the forcing projects predominantly on the dominant stochastic optimals, the angular momentum flux will be positive and of larger magnitude than that produced by unitary forcing. If the forcing projects predominantly on the higher order stochastic optimals, the angular momentum flux can become negative. Such a case can arise when the perturbation variance is maintained in a disk by a source with a particular structure, as for example in the case of convective turbulence, in which the structure is that of the buoyant plumes. In that case perturbations can grow from the unstable buoyancy gradients and need not utilize the shear energetics in order to maintain their variance. In such cases it may well happen that the stochastic forcing projects predominantly on the higher order stochastic optimals, presented in this paper, and the maintained angular momentum flux may be inward, as is indeed found in convection-dominated disks (Ryu & Goodman 1992; Gu 2000; Quataert & Chiang 2000).

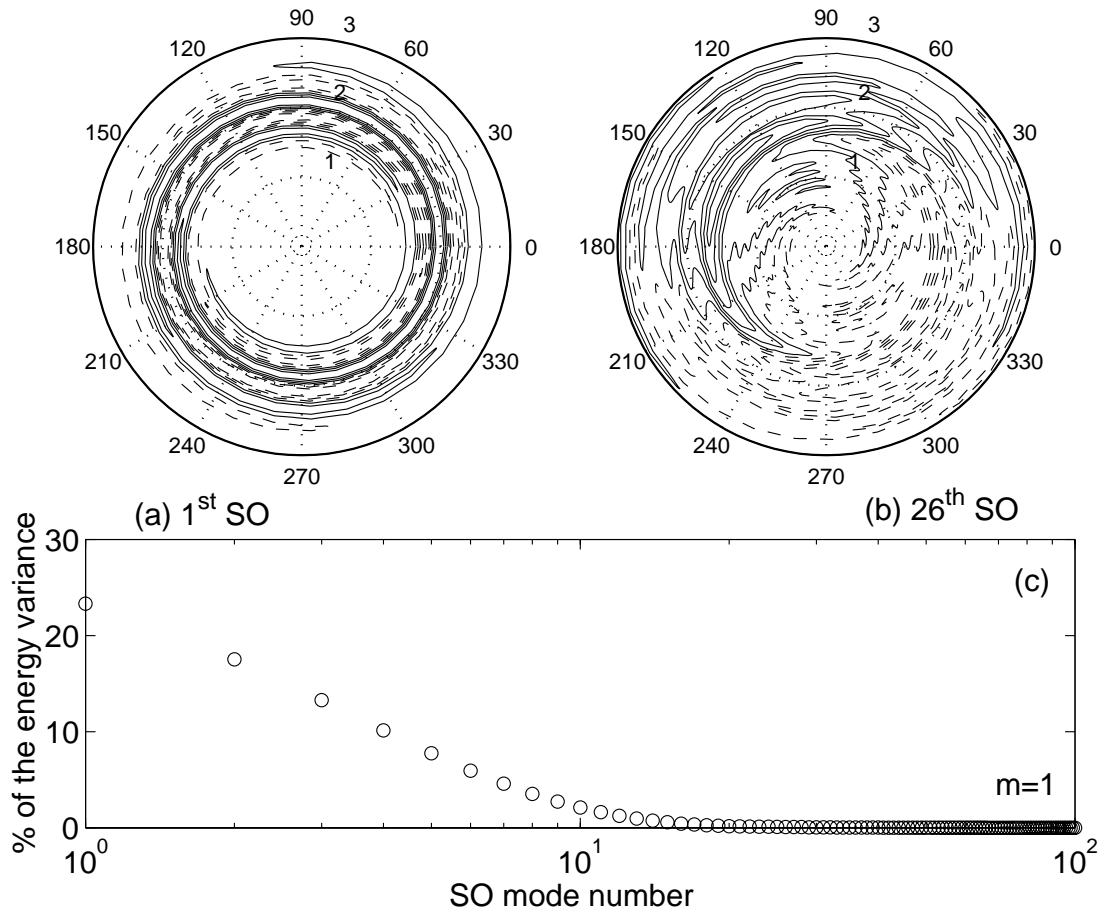


FIG. 9.—(a) Stream function of the first stochastic optimal (SO) for zonal $m = 1$ perturbations. This stochastic optimal is responsible for producing 23% of the mean variance. (b) The corresponding stream function of the 26th stochastic optimal for zonal $m = 1$ perturbations. This stochastic optimal is responsible for producing 0.09% of the mean variance. (c) Percentage ensemble mean energy produced by the first 100 stochastic optimals. The disk is Keplerian and extends from $r_1 = 0.1r_0$ to $r_2 = 3r_0$; the Reynolds number is $Re = 10^4$.

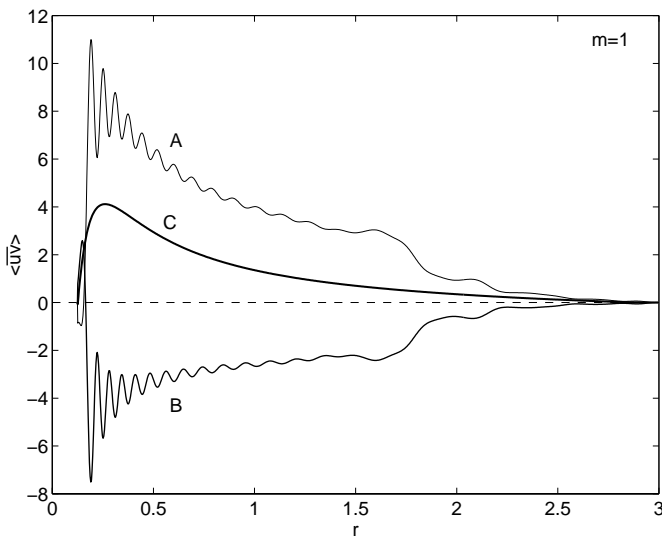


FIG. 10.—Radial distribution of the momentum flux for $m = 1$ perturbations in the statistical steady state for various forcings. (A) Forcing with only the first 25 stochastic optimals. (B) Forcing with the remaining stochastic optimals. (C) Forcing with all the stochastic optimals, in that case the forcing is unitary, i.e., $FF^\dagger = I$. The curve C is the sum of A and B. The disk is Keplerian and extends from $r_1 = 0.1r_0$ to $r_2 = 3r_0$; the Reynolds number is $Re = 10^4$.

In order for mass to accrete to the central gravitating body, the angular momentum flux must be positive throughout the disk. Spatially localized or temporally band-limited forcing, will in general be unable to extend its influence in the whole disk and produce positive momentum flux in the entirety of the disk, unless the forcing excites modal structures that do not have critical layers in the disk (Vishniac & Diamond 1989). In the disk model presented here all modes have viscous critical layers in the interior of the disk, and, consequently, the stochastic forcing can produce mass accretion if it is not systematically localized. For example, the angular momentum flux resulting from forcings localized in the inner, center, and outer region of the disk are shown in Figure 11. Note that for forcing localized in the outer region of the disk the angular momentum fluxes are concentrated around the radius that corresponds to the viscous critical layer associated with the phase speed of the least damped mode, which for the case shown is at $r_c \approx 4.7$.

We consider now monochromatic forcing at frequency ω . Taking the Fourier transform of equation (27) the amplitude of the perturbation response in generalized velocity coordinates is

$$\hat{z}(\omega) = \mathbf{R}(\omega)\hat{f}(\omega), \quad (43)$$

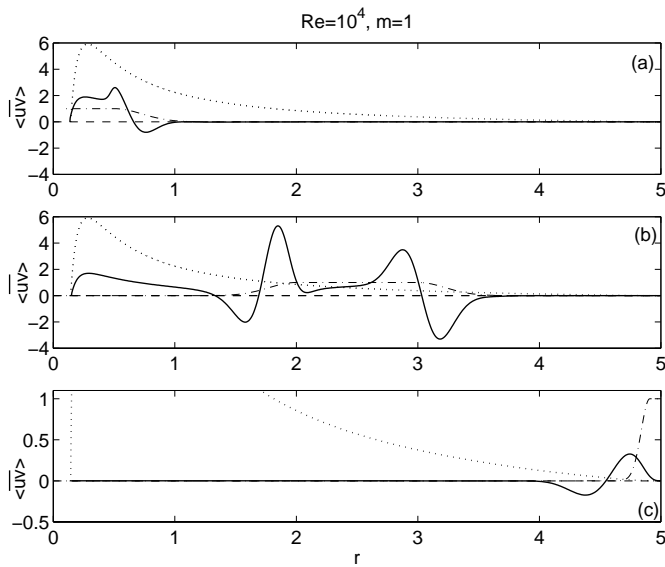


FIG. 11.—Radial distribution of the momentum flux (solid curve) for $m = 1$ perturbations in the statistical steady state for various forcings. (a) The forcing (dash-dotted curve) is limited to the inner region. The dotted line shows the momentum flux sustained under unitary forcing. (b) The forcing (dash-dotted curve) is limited to the central region of the disk. The dotted curve shows the momentum flux sustained under unitary forcing. (c) The forcing (dash-dotted curve) is limited to the exterior region of the disk. The dotted curve shows the momentum flux sustained under unitary forcing. In all cases the momentum flux is localized. The disk is Keplerian and extends from $r_1 = 0.1r_0$ to $r_2 = 5r_0$, the Reynolds number is $Re = 10^4$.

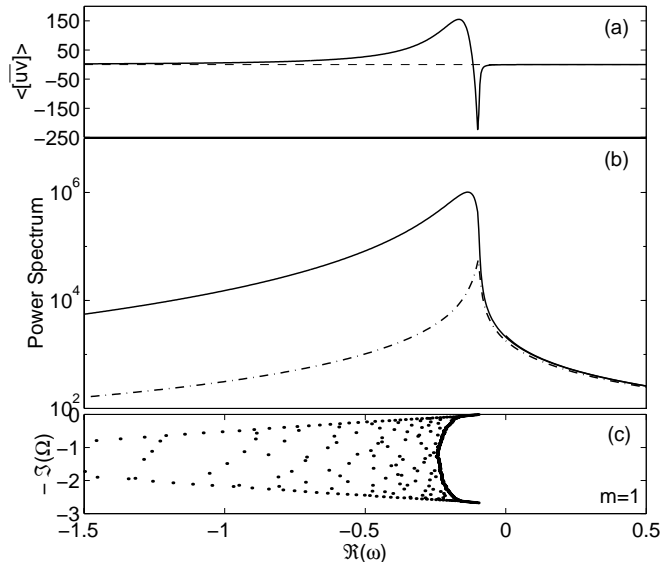


FIG. 12.—(a) Radially integrated momentum flux for $m = 1$ perturbations as a function of forcing frequency, ω . The forcing is distributed throughout the disk. The momentum flux is positive for almost all frequencies, except for frequencies that have critical layers in the vicinity of the outer radius of the disk, i.e., for frequencies $\omega \approx -m/r_2^{3/2}$, where r_2 is the outer radius of the disk. (b) The power spectrum of the perturbation energy as a function of frequency (solid line) and the power spectrum obtained as a summation of the contributions from the poles of the resolvent (dashed curve): $\sum_i 1/|i\omega - i\Omega_i|^2$, where $i\Omega_i$ are the eigenvalues of B , as it would be appropriate if B were a normal operator. The area under the curve of the energy power spectrum is the maintained ensemble mean perturbation energy. (c) The real $[\Re(\omega)]$ and the imaginary $[-\Im(\omega)]$ part of the eigenvalues of the operator B . The disk is Keplerian and extends from $r_1 = 0.1r_0$ to $r_2 = 5r_0$; the Reynolds number is $Re = 10^4$.

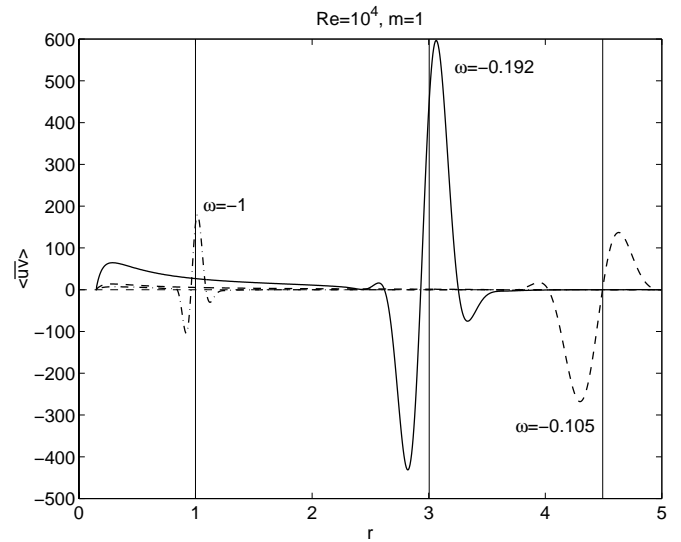


FIG. 13.—Radial distribution of the momentum flux for $m = 1$ perturbations for various forcing frequencies. The forcing is distributed throughout the disk. The momentum flux for forcing frequency $\omega = -1$ (dash-dotted curve), the critical layer (vertical line), is located at $r = 1$. The momentum flux for $\omega = -0.192$ (solid curve), the critical layer is at $r = 3$, and the momentum flux for forcing frequency $\omega = -0.105$ (dashed curve), with critical layer located at $r = 4.5$. In all cases the momentum flux is concentrated in the vicinity of the critical layer. The disk is Keplerian and extends from $r_1 = 0.1r_0$ to $r_2 = 5r_0$; the Reynolds number is $Re = 10^4$.

where the hat variables denote the Fourier amplitudes, i.e.,

$$\hat{z}(\omega) = \frac{1}{2\pi} \int_{-\infty}^{\infty} z(t) e^{-i\omega t} dt, \quad (44)$$

and $\hat{f}(\omega)$ is the Fourier amplitude of the forcing. The resolvent $R(\omega)$ determines the structure of the response and is given by

$$R(\omega) = (i\omega I - B)^{-1}. \quad (45)$$

We form the correlation matrix

$$C(\omega) = \hat{z}(\omega)\hat{z}^\dagger(\omega) = R(\omega)\hat{f}(\omega)\hat{f}^\dagger(\omega)R^\dagger(\omega), \quad (46)$$

and proceed to calculate the perturbation energy power spectrum, $P(\omega) = \text{trace}[C(\omega)]$, and angular momentum flux produced at each frequency as in the previous section. We will assume that the disk is forced equally at all radii and select $\hat{f}\hat{f}^\dagger = I$ and in this way determine the mean response of the disk at frequency ω to spatially uncorrelated forcing. The perturbation energy power spectrum and angular momentum flux as a function of frequency, ω , are shown in Figure 12. The angular momentum flux is positive for nearly all frequencies except for frequencies that have critical layers in the neighborhood of the outer radial boundary, i.e., for $\omega \approx -m/r_2^{3/2}$, where r_2 is the outer radius of the disk. The radial structure of the angular momentum fluxes at each frequency ω is concentrated around the corresponding critical layer located, for forcing frequency ω , at $r = (-m/\omega)^{2/3}$. The angular momentum flux is positive for nearly all frequencies except for frequencies that have critical layers in the neighborhood of the outer radial boundary, i.e., for $\omega \approx -m/r_2^{3/2}$, where r_2 is the outer radius of the disk. However, despite their positivity, the momentum fluxes are radially concentrated around the corresponding critical layer which is located, for forcing frequency ω , at $r = (-m/\omega)^{2/3}$. This is shown in Figure 13. Consequently, in

order to achieve mass accretion to the central body, it is additionally required that the forcing has a broad temporal spectrum.

6. CONCLUSION

The perturbation dynamics in Keplerian disks are governed by a nonnormal stable dynamical operator. In order to identify the perturbations that will dominate the perturbation structure and determine their second-order effects on the mean flow, the dynamics must be analyzed with the methods of generalized stability analysis. In this paper such a stability analysis of perturbation growth in Keplerian disks is presented under the simplifying assumption that the perturbation fields are nondivergent. We demonstrate that although the disk is asymptotically stable and perturbations eventually decay, there is robust rapid growth of a subset of optimal perturbations at the timescale of one rotational period of the disk. These transiently growing perturbations carry angular momentum outward during their growing phase, while in their decay phase they carry angular momentum inward. The perturbation growth was found to be dominated by zonal wavenumber $m = 1$ perturbations. We calculated the statistical steady state that emerges under white forcing in space and time. The perturbation structure was found to be organized by the non-normal mean operator into coherent structures that invariably export angular momentum outward. This shows

that when the full spectrum of perturbations are excited in the disk, their net effect is to transport angular momentum outward. Remarkably, the radial structure of the resulting angular momentum flux is very close to the one that is anticipated from equilibrium theory (Shakura & Sunyaev 1973; Pringle 1981; Balbus & Hawley 1998; Balbus & Papaloizou 1999). We have investigated the effect of spatial localization and temporal band limiting of the forcing, and it was found that the associated momentum fluxes will be spatially localized unless the forcing extends throughout the disk and is broadband. In conclusion, in the presence of distributed broadband forcing this work suggests that accretion in astrophysical Keplerian disks may proceed in the absence of exponential instabilities of the mean flow and may be explained by invoking only hydrodynamic processes.

It is intriguing that we succeeded in obtaining such a good angular momentum flux distribution under the simplified assumptions made in this paper. It suggests that the energy bearing perturbation structure in accretion disks may be dominated by essentially nondivergent motions rather than a sound field. This question is presently under investigation.

We thank Ethan Vishniac and Brian Farrell for their comments on the manuscript. Alexander Kakouris acknowledges the Greek National Scholarships Foundation for postdoctoral research financial support.

REFERENCES

- Balbus, S. A., & Hawley, J. F. 1991, *ApJ*, 376, 214
 ———. 1998, *Rev. Mod. Phys.*, 70, 1
 Balbus, S. A., Hawley, J. F., & Stone, J. M. 1996, *ApJ*, 467, 76
 Balbus, S. A., & Papaloizou, J. C. B. 1999, *ApJ*, 521, 650
 Chandrasekhar, S. 1960, *Proc. Natl. Acad. Sci.*, 46, 253
 DelSole, T. 1996, *J. Atmos. Sci.*, 53, 1617
 ———. 1999, *J. Atmos. Sci.*, 56, 3692
 Farrell, B. F. 1988, *Phys. Fluids*, 31, 2093
 Farrell, B. F., & Ioannou, P. J. 1993a, *Phys. Fluids A*, 5, 2600
 ———. 1993b, *J. Atmos. Sci.*, 50, 210
 ———. 1993c, *J. Atmos. Sci.*, 50, 4044
 ———. 1994, *Phys. Rev. Lett.*, 72, 1188
 ———. 1995, *J. Atmos. Sci.*, 52, 1646
 ———. 1996, *J. Atmos. Sci.*, 53, 2025
 ———. 1998, *Theor. Comput. Fluid Dyn.*, 11, 215
 ———. 1999a, *ApJ*, 522, 1079
 ———. 1999b, *ApJ*, 522, 1088
 Frank, J., King, A. R., & Raine, D. J. 1992, *Accretion Power in Astrophysics* (Cambridge: Cambridge Univ. Press)
 Godon, P. 1998, *ApJ*, 502, 382
 Goldreich, P., & Lynden-Bell, D. 1965, *MNRAS*, 130, 97
 Gu, P.-G. 2000, *ApJ*, 540, 404
 Hawley, J. F., Balbus, S. A., & Winters, W. F. 1999, *ApJ*, 518, 394
 Jaroszyński, M. 1988, *Acta Astron.*, 38, 289
 Li, H., Finn, J. M., Lovelace, R. V. E., & Colgate, S. A. 2000, *ApJ*, 533, 1023
 Lin, D. N. C., & Papaloizou, J. C. B. 1996, *ARA&A*, 34, 703
 Lovelace, R. V. E., Li, H., Colgate, S. A., & Nelson, A. F. 1999, *ApJ*, 513, 805
 Menou, K. 2000, *Science*, 288, 2022
 Nolan, D. S., & Farrell, B. F. 1999, *J. Atmos. Sci.*, 56, 1282
 Ohashi, N., & Hayashi, M. 1996, in *Disks and Outflows around Young Stars*, ed. S. Beckwith, J. Staude, A. Quetz, & A. Natta (Heidelberg: Springer), 48
 Papaloizou, J. C. B., & Lin, D. N. C. 1995, *ARA&A*, 33, 505
 Pringle, J. E. 1981, *ARA&A*, 19, 137
 Quataert, E., & Chiang, E. I. 2000, *ApJ*, 543, 432
 Ryu, D., & Goodman, J. 1992, *ApJ*, 388, 438
 Sargent, A. I., & Beckwith, S. V. W. 1991, *ApJ*, 382, L31
 Shakura, N. I., & Sunyaev, R. A. 1973, *A&A*, 24, 337
 Toomre, A. 1964, *ApJ*, 139, 1217
 ———. 1981, in *The Structure and Evolution of Normal Galaxies*, ed. S. M. Fall & D. Lynden-Bell (Cambridge: Cambridge Univ. Press), 111
 Vishniac, E. T., & Diamond, P. H. 1989, *ApJ*, 347, 435